# Refractive index sensor based on tapered PCF in-line interferometer

**Qi Liu (刘 奇)[1,2*] and Qin Wang (王 琴)[1,2]**

[1]*Department of Materials Science and Engineering, Nanjing University, Nanjing 210093, China*

[2]*Nanjing University High-Tech Institute at Suzhou, Suzhou 215123, China*

[*]*Corresponding author: lightnju@gmail.com*

Received January 6, 2012; accepted March 14, 2012; posted online July 5, 2012

A simple and compact refractive index sensor is demonstrated by tapering a photonic crystal fiber (PCF) in-line interferometer. The PCF is spliced between two single-mode fibers and tapered via hydrofluoric acid etching. Its sensitivity in liquid is more than an order of magnitude larger than the untapered one. By optimizing the etching process, we can fabricate more uniformly and thinly tapered PCF interferometers with higher sensitivity in the future.

*OCIS codes:* 060.5295, 060.2370, 120.3180, 280.4788.

*doi: 10.3788/COL201210.090601.*

Refractive index sensing is very important for chemical and biological applications because many substances can be detected through refractive index measurements. Optical fiber refractometers and refractive index sensors are attractive because of their small size, design flexibility, immunity to electromagnetic interference, network compatibility, and capability for remote and *in situ* measurements. To detect analytes, we have to design and process a fiber device to access the evanescent field. A considerable number of fiber-based refractive index sensors have been developed based on different technologies, such as D-shaped fiber devices[1,2], Bragg gratings based on tapered fibers[3−5], long-period fiber gratings[6,7], fiber Bragg grating[8], tilted fiber gratings[9−12], microfiber resonators[13−18], metal cladding tapered fibers[19], and photonic crystal fiber (PCF)-based interferometers[20]. PCF-based interferometers can be fabricated in many ways, and their properties and applications have been widely studied. Different types of PCF interferometers are mostly used in typical applications such as strain and temperature sensing[21−24]. Refractive index sensing for biological and chemical applications can also be realized using PCF interferometers. However, in most of these techniques, the samples have to be infiltrated into the holes of the PCF. Moreover, the PCF is tens of centimeters long and has a poor response rate. Recently, a simple and compact PCF interferometer built via fusion splicing has been reported and has attracted much attention[25,26]. This device is composed of a stub of 125 $\mu$m large-mode-area (LMA) PCF spliced between the same size standard single-mode fibers (SMFs)[25,26]. The air holes of the PCF are tapered because of the high-strength fusion splices. Then, they are completely converted into a solid piece of silica over a short region, allowing the coupling and recombination of the PCF core and cladding modes. This in-line PCF modal interferometer is fit for refractive index sensing measurements through the interaction of the evanescent field and the analyte samples in the outer region of the PCF section because the cladding mode is sensitive to the outside environment. Moreover, the device fabrication is very simple because it only involves cleaving and splicing processes, which can be performed in a standard fiber optics laboratory[25,27]. The device is cost-efficient, highly stable over time, and needs only a small cheap commercial LMA PCF of standard size[25,27]. It does not need complex polarimetric devices using expensive polarization to maintain the PCF[7]. In addition, the samples do not need to be infiltrated into the holes of the PCF, which is very short and whose response rate is good. However, the limited evanescent field caused by the large fiber size makes the refractive index sensitivity of this kind of sensor low. To enlarge the available evanescent field and increase sensitivity, we fabricated a miniature tapered PCF interferometer with enhanced sensitivity via the etching method[28]. We did not use the conversational heat-and-draw technology[29] to taper the PCF because it significantly elongated the PCF length. Moreover, preventing the holes from collapsing while maintaining the interference properties during the tapering of the small PCF was difficult. We theoretically and experimentally investigated the refractive index sensing properties after and before the tapering process. After tapering, the size decreased and the refractive index sensitivity increased more than ten times. The entire sensor size was only several millimeters in length and tens of micrometers in diameter. By optimizing the tapering process, we can fabricate more thinly tapered PCF interferometers with higher sensitivity in the future.

A commercial endless single-mode PCF (LMA-8, NKT Photonics) was used to fabricate the SMF-PCF-SMF in-line interferometer. As shown in Fig. 1(a), this PCF consists of a solid core surrounded by six rings of air holes arranged in a hexagonal pattern. The core diameter was ~8.4 $\mu$m, the average diameter of air holes was ~2.2 $\mu$m, and the average pitch (hole-to-hole distance) was ~5.3 $\mu$m. In contrast to other larger PCFs, the LMA-8 PCF has the same diameter as that of SMF-28 fibers. Moreover, it is easier and cheaper to splice than SMF-28 fibers and has better repetition and higher stability.

To fabricate the PCF interferometer, we first spliced the ends of the two SMF-28 fibers to a few millimeters of the cleaved end of the PCF using a commercial fusion splicer. The air holes of the PCF were tapered because

 © 2012 Chinese Optics Letters

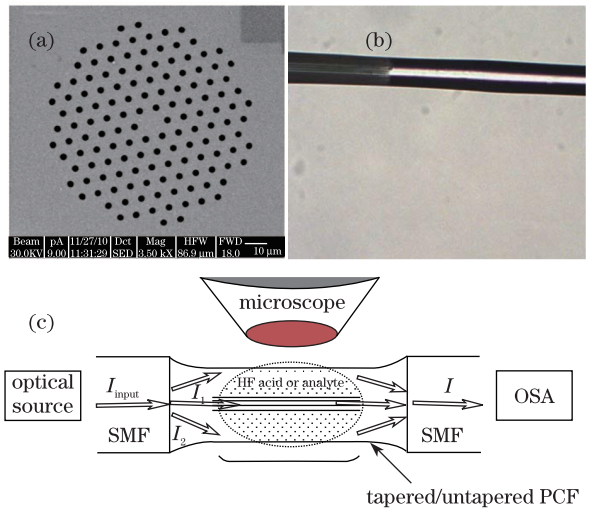


Fig. 1. (a) Scanning electron microscope image of the cross section of the PCF (LMA-8) used in the experiment; (b) splicing region between the PCF and SMF after ∼30 min of etching; (c) schematic of the experimental setup for etching and measuring the refractive index sensitivity.

of the high-strength fusion splices. Then, they were converted completely into a solid piece of silica over a short region about several hundreds of micrometers long. To minimize the losses and achieve robust splices, we reduced the default (for standard SMF) heating time and current of the electrodes of the splicer[27]. Thereafter, we etched the PCF interferometer using hydrofluoric (HF) acid. We dropped an acid microdroplet with 40% HF onto the dish, and the dish was lifted by a translation stage to immerse the fiber into the droplet and begin the etching process. We can control the length of the waist region by adjusting the immersion depth of the PCF. The tapered PCF was monitored using a microscope in real time and *in situ* during etching. In our experiment, the device was held by two clamps across a HF-resistant dish to keep the PCF straight. It was placed on an optical table to maintain the mechanical stability, and the whole experiment process was performed at room temperature. The etching velocity was ∼2 $\mu$m/min for the thinnest waist of the tapered PCF in our experimental environment. Figure 1(b) shows the splicing region between the PCF and SMF after 30 min of etching. The thinner waist of the tapered PCF was about ∼60 $\mu$m. The fabrication reproducibility depended on the precise control of the PCF length and splicing, which strongly relied on the performance of the fabrication facilities, particularly the splicer. Using the best splicer will achieve good reproducibility.

The SMF fundamental mode began to diffract when the light was transmitted from the SMF to the tapered PCF (Fig. 1(c)) in the interferometer. It excited the core and cladding modes in the PCF section with different propagation constants upon entering the collapsed PCF region[8,11,12]. After accumulating a phase difference along the PCF, the modes further diffracted and recombined through the filtering of the subsequent SMF. Therefore, the interference spectrum can be expressed using the following two-beam optical interference equation:

$$I = I_1 + I_2 + 2\sqrt{I_1 I_2}\cos(2\pi\Delta n_{\rm eff}L/\lambda), \qquad (1)$$

$$\text{free spectral range (FSR)} = \lambda^2/(\Delta n_{\rm eff}L), \qquad (2)$$

where $I$ is the intensity of the total interference signal; $I_1$ and $I_2$ are the intensities of the cladding and core modes, respectively; $\Delta n_{\rm eff}$ is the difference between the effective refractive indices of the core ($n_{\rm co}$) and cladding ($n_{\rm cl}$) modes, which depend on the local diameter $D$ of the tapered PCF if the taper is not uniform; $\lambda$ is the wavelength; $L$ is the length of the PCF section.

The transmission spectra response of the PCF interferometer was measured in real time using a broadband amplified spontaneous emission (ASE) source and an optical spectrum analyzer (OSA, Ando AQ6317B), as shown in Fig. 1(c). In our experiment, a PCF of about 1 cm was spliced between two SMFs. Then, we etched the PCF with 40% HF acid. Before measuring the spectra, we removed the HF acid and cleaned and dried the PCF in air. Then, we measured the transmission spectra in air, isopropanol, acetone, and mixtures of isopropanol and acetone, respectively.

Figure 2 shows the measured transmission spectra of the PCF interferometer before and after tapering in air. The FSR was large (∼ 45 nm) before tapering because of the ultra-short PCF. This result is similar to the theoretical result (∼ 48 nm from Eq. (2)). The extinction ratio was ∼13 dB before tapering. Both the FSR and extinction ratio increased after tapering, possibly because more energy was excited to the cladding mode with the smaller $n_{\rm cl}$.

The stability of an interferometer over time is important for sensing applications. Our sensor is only made of silica, and the whole device is assembled by permanent and strong splicing. Thus, high stability over time is expected. In fact, the excellent stability of this kind of PCF interferometer was tested and demonstrated in Ref. [30], and it did not degrade over a long period of time.

Another important issue is temperature stability. The temperature sensitivity of this is always very low as the PCF is made of silica and air with low thermo-optic and thermal expansion coefficients. The temperature sensitivity is smaller than 10 pm/°C. The excellent stability of this kind of PCF interferometer was tested and demonstrated in Ref. [30], and it did not degrade at high temperatures.

The interference pattern is not very regular possibly because of the nonuniform mode excitation coefficient in the splicing region and the leaky loss of cladding modes.

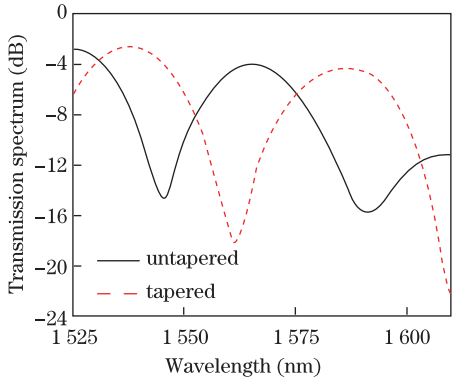


Fig. 2. Transmission spectra of the PCF interferometer before and after tapering in air.

The operational wavelength range of our ASE source is only the C+L band. We can expect that the interference pattern looks similar around 1 310 nm but with different extinction ratios and FSRs. However, for our sensing application, we only need to monitor one peak/valley. Thus, the C+L band optical source is enough for our application.

The performance of resonant or interferometer refractive index sensors can be evaluated using sensitivity $S$, which is defined as the magnitude in the shift of the resonant wavelength divided by the change in the refractive index of the analyte. When the untapered/tapered PCF is surrounded by certain analyte samples ($n_a$), $n_{cl}$ changes with $n_a$ because of the interaction between the evanescent field of the cladding mode and analyte samples. Then, the interference wavelength shifts. In our experiment, $n_{co}$ is constant because the core mode is isolated from the outside environment when $D$ is large. The refractive index sensitivity $S$ is the interference wavelength ($\lambda_i$) shift divided by the corresponding $n_a$ change

$$S = \frac{d\lambda_i}{dn_a} = \frac{\lambda_i}{n_{cl} - n_{co}} \frac{\partial(n_{cl} - n_{co})}{\partial n_a}. \quad (3)$$

The sensitivity of the device was measured by immersing the PCF section into isopropanol and acetone mixtures. The refractive indices of pure isopropanol and acetone at 1.55 $\mu$m were 1.3739 and 1.3577, respectively[31]. These solutions were chosen to simulate aqueous solutions having a refractive index of around 1.33 in the region at a wavelength of $\lambda$=1.55 $\mu$m. The aqueous solutions were dropped on a plate, and the plate was lifted by a translation stage to immerse the fiber. The tapered/untapered PCF interferometer did not have to be moved and re-fixed in the whole experiment, which was very useful because it avoided the influence of bending and twisting. The interferometer worked in transmission and did not use any fiber optic circulator, as reported in Ref. [32]. In addition, the device was easy to clean and re-use compared with other fiber sensors with inside or side open holes for liquid or gas access.

Figure 3 shows the spectra of the untapered PCF interferometer when immersed in the acetone and isopropanol mixtures of 20%, 40%, and 80% isopropanol, respectively. The extinction ratio was about ~ 12 dB. They shifted to red when the outer environment changed with increasing isopropanol percentage.

Figures 4 shows the relationship between the outer liquid refractive indices and the wavelength shift of the PCF interferometer after and before tapering. The refractive index sensitivity of the untapered PCF interferometer was about ~49 nm/RIU. After tapering, the sensitivity reached ~500 nm/RIU, which is an order of magnitude larger than the result of the untapered PCF interferometer and much higher than the previous results of this kind of PCF interferometer. The thinner waist of the tapered PCF was about ~60 $\mu$m after 30 min of etching, and several air holes at the edge of air rings were etched. Higher sensitivity (~100 times larger than an untapered PCF interferometer) can be realized theoretically with more uniformly and thinly tapered PCFs, which can be achieved by optimizing the etching process.

In conclusion, we fabricate a highly sensitive tapered PCF interferometer via HF acid etching. It is an in-line

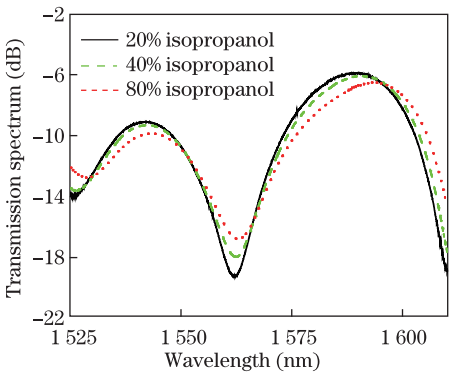


Fig. 3. (Color online) Transmission spectra of the untapered PCF interferometer when immersed in different liquids.

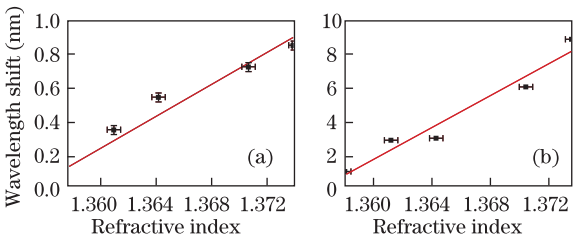


Fig. 4. Dependence of the measured wavelength shift on the liquid refractive index (a) before and (b) after tapering. The asterisk represents the measured results, whereas the solid line indicates the linear fitting result.

modal interferometer based on the interference among the core and excited cladding modes. We experimentally investigate the refractive index sensing properties before and after tapering. As the size decreased, the sensitivity significantly increases (> 10 times; ~500 nm/RIU) after ~30 min of etching.

This work was supported by the National "973" Program of China (No. 2010CB327800), the Natural Science Foundation of Jiangsu Province of China (No. BK2010247), and the Priority Academic Program Development of Jiangsu Higher Education Institutions.

## References

1. J.-L. Kou, Z.-D. Huang, G. Zhu, F. Xu, and Y.-Q. Lu, Appl. Phys. B: Lasers Opt. **102,** 615 (2011).
2. M. Yang, J. Dai, X. Li, and J. Wang, J. Appl. Phys. **108,** 033102 (2010).
3. F. Xu, G. Brambilla, J. Feng, and Y. Lu, IEEE Photon. Technol. Lett. **22,** 218 (2010).
4. F. Xu, G. Brambilla, and Y. Lu, Opt. Express **17,** 20866 (2009).
5. W. Liang, Y. Huang, Y. Xu, R. K. Lee, and A. Yariv, Appl. Phys. Lett. **86,** 151122 (2005).
6. V. Bhatia, Opt. Express **4,** 457 (1999).
7. J. H. Chong, P. Shum, H. Haryono, A. Yohana, M. K. Rao, C. Lu, and Y. Zhu, Opt. Commun. **229,** 65 (2004).
8. Y. Cao, Y. Yang, X. Yang, and Z. Tong, Chin. Opt. Lett. **10,** 030605 (2012).
9. C. Caucheteur, D. Paladino, P. Pilla, A. Cutolo, S. Campopiano, M. Giordano, A. Cusano, and P. Megret, IEEE Sensor J. **8,** 1330 (2008).
10. G. Laffont and P. Ferdinand, Meas. Sci. Technol. **12,** 765 (2001).

11. G. Tuan, C. Chengkun, A. Laronche, and J. Albert, IEEE Photon. Technol. Lett. **20,** 635 (2008).
12. C. Caucheteur and P. Megret, IEEE Photon. Technol. Lett. **17,** 2703 (2005).
13. F. Xu and G. Brambilla, Appl. Phys. Lett. **92,** 101126 (2008).
14. F. Xu, P. Horak, and G. Brambilla, Opt. Express **15,** 9385 (2007).
15. F. Xu, P. Horak, and G. Brambilla, Opt. Express **15,** 7888 (2007).
16. F. Xu, V. Pruneri, V. Finazzi, and G. Brambilla, Opt. Express **16,** 1062 (2008).
17. X. Guo and L. Tong, Opt. Express **16,** 14429 (2008).
18. S. S. Pal, S. K. Mondal, U. Tiwari, P. V. G. Swamy, M. Kumar, N. Singh, P. P. Bajpai, and P. Kapur, Rev. Sci. Instrum. **82,** 095107 (2011).
19. J.-L. Kou, S.-J. Qiu, F. Xu, Y.-Q. Lu, Y. Yuan, and G. Zhao, IEEE Photon. Technol. Lett. **23,** 1712 (2011).
20. J. Villatoro, M. P. Kreuzer, R. Jha, V. P. Minkovich, V. Finazzi, G. Badenes, and V. Pruneri, Opt. Express **17,** 1447 (2009).
21. T. M. Monro, W. Belardi, K. Furusawa, J. C. Baggett, N. G. R. Broderick, and D. J. Richardson, Meas. Sci. Technol. **12,** 854 (2001).
22. G. Kim, T. Cho, K. Hwang, K. Lee, K. S. Lee, Y.-G. Han, and S. B. Lee, Opt. Express **17,** 2481 (2009).
23. S.-S. Li, X.-S. Song, F. Xu, and Y.-Q. Lu, Electron. Lett. **47,** 719 (2011).
24. S.-J. Qiu, Y. Chen, F. Xu, and Y.-Q. Lu, Opt. Lett. **37,** 863 (2012).
25. R. Jha, J. Villatoro, G. Badenes, and V. Pruneri, Opt. Lett. **34,** 617 (2009).
26. J. Villatoro, V. P. Minkovich, V. Pruneri, and G. Badenes, Opt. Express **15,** 1491 (2007).
27. J. Villatoro, V. P. Minkovich, V. Pruneri, and G. Badenes, Opt. Express **15,** 1491 (2007).
28. E. J. Zhang, W. D. Sacher, and J. K. S. Poon, Opt. Express **18,** 22593 (2010).
29. V. P. Minkovich, J. Villatoro, D. Monzon-Hernandez, S. Calixto, A. B. Sotsky, and L. I. Sotskaya, Opt. Express **13,** 7609 (2005).
30. R. Jha, J. Villatoro, and G. Badenes, Appl. Phys. Lett. **93,** 191106 (2008).
31. J.-L. Kou, J. Feng, Q.-J. Wang, F. Xu, and Y.-Q. Lu, Opt. Lett. **35,** 2308 (2010).
32. S.-Y. Zhang, Q. Zhong, X.-S. Qian, X.-W. Lin, F. Xu, W. Hu, and Y.-Q. Lu, J. Appl. Phys. **108,** 023107 (2010).